THE ASTROPHYSICAL JOURNAL, 402:694–709, 1993 January 10

GODDARD HIGH-RESOLUTION SPECTROGRAPH OBSERVATIONS OF THE LOCAL INTERSTELLAR MEDIUM AND THE DEUTERIUM/HYDROGEN RATIO ALONG THE LINE OF SIGHT TOWARD CAPELLA[1]

JEFFREY L. LINSKY,[2,3] ALEXANDER BROWN,[3] KEN GAYLEY,[3] ATHANASSIOS DIPLAS,[4] BLAIR D. SAVAGE,[4]
THOMAS R. AYRES,[5] WAYNE LANDSMAN,[6] STEVEN N. SHORE,[6] AND SARA R. HEAP[7]

Received 1992 April 23; accepted 1992 July 16

ABSTRACT

We analyze *HST* Goddard High-Resolution Spectrograph observations of the 1216, 2600, and 2800 Å spectral regions for the spectroscopic binary system Capella, obtained at orbital phase 0.26 with 3.27–3.57 km s^{-1} resolution and high signal-to-noise ratio. We infer the column densities of H I, D I, Mg II, and Fe II for the local interstellar medium along this 12.5 pc line of sight, together with estimates of the temperature and turbulent velocity. If we assume that the intrinsic Lyα lines of the component stars in the Capella system can be approximated as scaled solar lines (with self-reversals), which is consistent with the observed Lyα profile of the high radial velocity star δ Lep, then the interstellar neutral hydrogen column density toward Capella, $N_{\rm H\,I} = 1.80(\pm 0.1) \times 10^{18}$ cm^{-2}. This corresponds to an average hydrogen number density, $n_{\rm H\,I} = 0.047$ cm^{-3}. To account for a wider range of intrinsic line profiles that may characterize the more active Capella stars, we increase the allowed range of $N_{\rm H\,I}$ to $1.8(+0.3, -0.1) \times 10^{18}$ cm^{-2}. The deuterium column density and line width parameter are found to be $N_{\rm D\,I} = 2.97(+0.13, -0.05) \times 10^{13}$ cm^{-2} and $b_{\rm D} = 7.81(+0.23, -0.03)$ km s^{-1}. The widths of the interstellar D I, Mg II, and Fe II lines indicate that the broadening has both thermal and turbulent components with the temperature $T = 7000 \pm 200$ K, and the turbulent velocity $\xi = 1.66 \pm 0.03$ km s^{-1}. These parameters indicate that $b_{\rm H\,I} = 10.9$ km s^{-1}. We infer that the atomic deuterium/hydrogen ratio by number is $(\rm D/H)_{LISM} = 1.65(+0.07, -0.18) \times 10^{-5}$ for this line of sight.

Our value of the D/H ratio lies near the mean of many earlier but less certain values for the Capella line of sight and toward other stars located as far as 1 kpc from the Sun. We present evidence that a constant value for $(\rm D/H)_{LISM}$ in the nearby Galactic disk should be adopted as the best available working hypothesis, but this hypothesis must be tested by future *HST* observations of Capella at phase 0.75 and of other stars. Galactic evolution calculations indicate that the primordial D/H ratio, $(\rm D/H)_p$, probably lies in the range of (1.5–3) $\times$ $(\rm D/H)_{LISM}$. Standard big bang nucleosynthesis models for $(\rm D/H)_p = 2.2$–2.5×10^{-5} imply that $\Omega_B h_{50}^2 = 0.06$–0.08, where Ω_B is the baryonic density in units of the Einstein-de Sitter closure density, and h_{50} is the Hubble constant in units of 50 km s^{-1} Mpc^{-1}. If $H_0 = 80$ km s^{-1} Mpc^{-1} as recent evidence suggests, then $\Omega_B = 0.023$–0.031. Thus the universe will expand forever, unless nonbaryonic matter greatly exceeds the amount of baryonic matter.

Subject headings: ISM: abundances — stars: individual (α Aurigae) — ultraviolet: interstellar

1. INTRODUCTION

Analysis of ultraviolet spectra obtained with the *Copernicus*, *IUE*, and *Voyager* spacecraft and ground-based high-resolution optical spectra has provided estimates of the properties of the interstellar gas located within 50 pc of the Sun. We refer to this region as the local interstellar medium or LISM. Analyses of these data by Frisch & York (1983), Bruhweiler (1984), Paresce (1984), and Bruhweiler & Vidal-Madjar (1987) place the Sun near the edge of a warm cloud with $n_{\rm H\,I} \sim 0.1$ cm^{-3} and $T \sim 10^4$ K. This partially ionized cloud has appreciable neutral hydrogen column density, $N_{\rm H\,I} \sim 10^{19}$ cm^{-2}, toward the Galactic center, but $N_{\rm H\,I} \approx 10^{18}$ cm^{-2} or even lower in other directions. Surrounding the local cloud is the "Local Bubble" consisting of tenuous ($n_{\rm H\,I} \approx 0.001$–$0.01$ cm^{-3}), hot ($T \leq 10^6$ K) plasma that extends at least another 50 pc.

Several data sets provide additional information concerning the complexity of the LISM. Crutcher (1982) finds that the local cloud has a bulk flow of 28 km s^{-1} relative to the local standard of rest from the direction of the Sco-Cen association, but Lallement, Vidal-Madjar, & Ferlet (1986) found that this general flow breaks up into at least four identifiable velocity components toward nearby stars and that three of these components lie in the line of sight toward Altair, which is only 5 pc distant (Ferlet, Lallement, & Vidal-Madjar 1986). Furthermore, there are some lines of sight with extremely low densities, such as the "interstellar tunnel" toward β CMa for which $N_{\rm H\,I} \leq 2.4 \times 10^{18}$ cm^{-2} along this 200 pc line of sight on the basis of Na I observations (Welsh 1991) and $N_{\rm H\,I} = 1$–2.2×10^{18} cm^{-2} on the basis of *Copernicus* observations of the Lyβ and Lyγ lines (Gry, York, & Vidal-Madjar 1985). This corresponds to a mean density of $n_{\rm H\,I} \leq 0.004$ cm^{-3}. This very low density line of sight was first identified by Bohlin, Savage,

[1] Based on observations with the NASA/ESA *Hubble Space Telescope*, obtained at the Space Telescope Science Institute, which is operated by the Association of Universities for Research in Astronomy, Inc., under NASA contract NAS5-26555.

[2] Staff Member, Quantum Physics Division, National Institute of Standards and Technology.
[3] Joint Institute for Laboratory Astrophysics, University of Colorado and National Institute of Standards and Technology, Boulder, CO 80309-0440.
[4] Astronomy Department, University of Wisconsin, Madison, WI 53706.
[5] Center for Astrophysics and Space Astronomy, University of Colorado, Boulder, CO 80309-0389.
[6] Hughes/STX, Code 681, NASA/Goddard Space Flight Center, Greenbelt, MD 20771.
[7] Code 681, NASA/Goddard Space Flight Center, Greenbelt, MD 20771.

& Drake (1978) using *Copernicus* observations of the Lyα line, and Welsh determined its angular extent on the sky and its geometry as an extension of the Local Bubble. Cox & Reynolds (1987) have described the physical processes that are likely to be responsible for the hot gas and clouds in the LISM.

Ultraviolet absorption spectroscopy of the interstellar gas toward nearby stars also provides a powerful technique for measuring the present value of the deuterium abundance in the disk of the Galaxy. The local D/H ratio, $(D/H)_{LISM}$, provides important constraints on the chemical evolution of the Galaxy and theories of big bang nucleosynthesis. In particular, the primordial D/H ratio, $(D/H)_p$, which can be estimated from $(D/H)_{LISM}$, is one of the few available measures of the baryon density of the universe, which with the uncertain density of nonbaryonic dark matter, determines whether the universe is open or closed.

In this paper we report the first in a series of observations of local stars with the *Hubble Space Telescope* Goddard High-Resolution Spectrometer (GHRS). These observations are designed to refine our understanding of the LISM and to measure the deuterium abundance along several very different lines of sight. The high spectral resolution ($\lambda/\Delta\lambda \approx 90{,}000$) and signal-to-noise ratio (S/N) (exceeding 100 for some spectra) of the GHRS echelle data resolve the ultraviolet interstellar line profiles for these lines of sight for the first time. This permits us to analyze the line profiles directly, rather than by using equivalent widths and curve-of-growth techniques that are less accurate. Our data allow us to determine much more accurate column densities for lines such as deuterium Lyα than heretofore possible. Also, the high spectral resolution of our data permits us to analyze accurately the damping wings of the hydrogen Lyα absorption. When $N_{H\,I} \leq 4 \times 10^{18}$ cm^{-2} (cf. McClintock et al. 1978), the interstellar Lyα line of atomic deuterium can be detected at -81.6 km s^{-1} (-0.3307 Å) from the interstellar Lyα line of atomic hydrogen.

2. GHRS OBSERVATIONS AND REDUCTIONS

2.1. *Observations*

We have observed Capella with the GHRS between 02:20 and 13:56 UT on 1991 April 15. The observations analyzed in this paper are summarized in Table 1. A subsequent paper will describe our analysis of the lower dispersion observations of the emission lines formed in the chromospheres and transition regions of the Capella system stars that were obtained at the same time. For a description of the GHRS see Brandt et al. (1982) and Duncan (1992). For a discussion of the prelaunch measured properties of the GHRS echelle gratings see Cardelli, Ebbets, & Savage 1990).

The echelle mode spectra were obtained with the stellar image in the small science aperture (SSA) and have spectral resolutions, $\lambda/\Delta\lambda$, ranging from approximately 84,000 to 92,000. The Digicon substepping pattern 9 was used for the echelle A measurements of the D I and H I lines. Pattern 7 was used for the echelle B measurements of the Fe II and Mg II lines. Substep patterns 7 and 9 each provide four spectral samples per Digicon diode width. Pattern 9 samples the background with the large corner background diodes, while pattern 7 also samples the background with the full 500 diode array positioned above and below the echelle order of interest. The G140L spectrum that includes the Lyα line was obtained in the large science aperture (LSA). Because of the *HST* spherical aberration, these data have a degraded spectral resolution of approximately 1000. The G140L data were obtained with substep pattern 5 (see Duncan 1992).

Four position comb-addition (see Duncan 1992), which reduces the effects of diode-to-diode sensitivity variations, was used for all measurements. The echelle A measurements were also obtained with the procedure FP-SPLIT = 4, which is intended to reduce photocathode fixed pattern noise and granularity. In this procedure the GHRS grating carousel is moved in order to obtain spectra at four different positions on the Digicon detector. The on-board Doppler compensation to correct for the changing spacecraft radial velocity was enabled during all observations.

2.2. *Reductions*

The processing of the spectra employed the 1991 December version of the CALHRS calibration software at the GHRS computing facility at the Goddard Space Flight Center. The processing includes converting raw counts to count rates, correcting for paired pulse events and diode-to-diode nonuniformities. The quarter-diode stepped spectra are merged to form the individual spectra of 2000 wavelength samples. The final reduction includes proper alignment of the individual FP-SPLIT spectra, rejection of fixed pattern noise structures, correction for scattered light and the radiation background, and wavelength calibration including the effects of thermal drifts.

The individual FP-SPLIT spectra obtained for the echelle A spectra were aligned and merged. Precise alignment was achieved through a centroiding procedure with reference to the interstellar line of D I. A fixed pattern noise structure was apparent for two of the FP-SPLIT positions corresponding to the wavelength region from approximately 1215.5 to 1215.6 Å. In the other two FP-SPLIT positions the feature was situated in the core of the H I Lyα line and did not contaminate the data. During the final merging of the four individual FP-SPLIT spectra, the effects of this fixed pattern noise structure were removed by replacing the corrupted data in the region of the feature with an average of the results obtained from the two FP-SPLIT alignments unaffected by the fixed pattern structure. The merged echelle A spectrum is shown in Figure 1.

TABLE 1

SUMMARY OF GHRS OBSERVATIONS

Grating	Aperture and Substep Pattern	Spectral Range	Spectral Resolution		Exposure Time (s)	Start Time (UT)	Important Spectral Features
			$\lambda/\Delta\lambda$	km s^{-1}			
EA-46	SSA 9	1211–1217 Å	84030	3.57	3917	10:04	H I + D I 1216 Å
EB-22	SSA 7	2594–2606 Å	91740	3.27	707	13:37	Fe II 2599 Å
EB-20	SSA 7	2793–2807 Å	84750	3.54	707	13:23	Mg II 2796, 2803 Å
G140L	LSA 5	1161–1449 Å	1000	300	25.6	07:05	H I, C II, Si IV, etc.

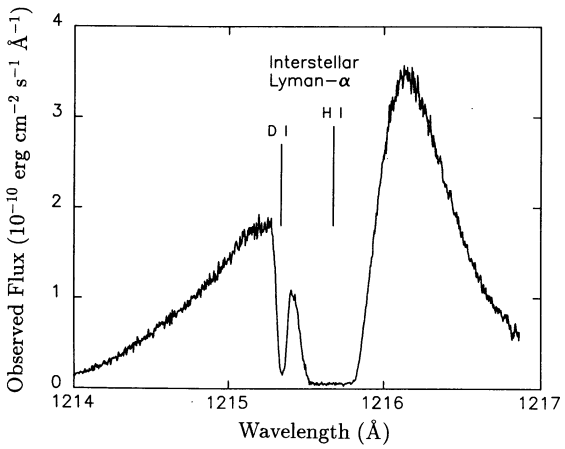

FIG. 1.—High-dispersion ($\lambda/\Delta\lambda = 84{,}000$) spectrum of the 1216 Å region obtained with the echelle A grating. The profile consists of a broad Lyα emission line produced in the chromospheres of both stars and absorption by interstellar hydrogen and deuterium ($\Delta\lambda = -0.33$ Å relative to hydrogen) along the 12.5 pc line of sight to Capella. In this presentation the residual scattered light in the core of the Lyα line has not been removed.

For the echelle B measurements the background correction was determined by fitting a third-order polynomial to the average interorder background recorded by the diode array and subtracting this from the gross spectrum to produce a net spectrum. This procedure removes the radiation background and most of the scattered light background. However, an additional scattered light correction was applied following the recommended procedures of Cardelli et al. (1990) and Cardelli, Savage, & Ebbets (1991b). This additional correction was 2.5% of the net average spectrum for the Fe II 2600 Å measurement and 1.5% of the average net spectrum for the Mg II 2800 Å measurement.

For the echelle A data the net spectrum was determined by making two corrections to the raw data. First, the average background was measured by the corner background diodes and linearly interpolating across the diode array. Figure 1 shows the Lyα line after this correction. Second, the additional scattered light background was estimated from the residual intensity found in the core of the strongly saturated H I interstellar Lyα absorption (see Fig. 1). However, the assumption that the background is constant with wavelength produces a negative spectrum in the far wings of the Lyα emission near 1212.0 Å. From the work of Cardelli et al. (1990), a change in the scattered light level with wavelength would be expected. The final background adopted includes a linear increase over the wavelength interval 1212.0 to 1216.8 Å, which is selected to make both the final level near 1212.0 Å and in the core of the interstellar Lyα absorption equal to zero. The adopted backgrounds at the positions of the centers of the D I and H I Lyman lines are 11.38% and 11.97% of the net average spectrum, respectively.

Wavelength calibration using the CALHRS reduction software as of 1991 December was performed with the special platinum lamp calibration exposures obtained for each of the echelle mode observations immediately before each stellar integration. There is not substantial GHRS observing experience to provide information about the improvement in accuracy of wavelength calibrations when special platinum lamp calibration measurements are obtained. However, there is information on the expected accuracy for carefully processed data involving no additional wavelength calibration. In their study of interstellar absorption toward ζ Oph, Cardelli et al. (1991b) find a dispersion of 2.2 km s^{-1} about the average velocity expected for narrow interstellar absorption lines for carefully processed data which include allowance for thermal drifts in the spectrograph. The ζ Oph spectrum contains three interstellar Mn II lines in echelle A order 47, the order adjacent to that used for observing the Capella Lyα lines, which have laboratory wavelengths of 1197.184, 1199.391, and 1201.118 Å. The relative errors in the measured wavelengths of these lines correspond to a relative velocity error of 1.0 km s^{-1}, indicating a possible error in the dispersion relation for this order of approximately 0.1%. These results suggest the magnitude of the wavelength errors we might expect in the Capella data.

Uncertainties associated with the centering of the stellar image in the 0.″25 × 0.″25 aperture will influence the wavelength calibration. The spectrograph entrance aperture size corresponds to 3.5 km s^{-1} at the detector, and slight changes in the position of the image could introduce velocity uncertainties of perhaps $\frac{1}{4}$ of the aperture size or about 1 km s^{-1}. Another problem is the sensitivity of the electron deflection system of the echelle A Digicon 1 to the motion through the magnetic field of the Earth. Imprecision in correcting for this effect may also introduce wavelength errors. The expected 1 σ error associated with the wavelength calibration of the Capella echelle mode data is estimated to be approximately 1.5 km s^{-1}. The results we have obtained for interstellar line velocities, which are listed in Tables 2 and 3 and discussed in § 3, are consistent with this expected calibration error.

3. ANALYSIS

We observed the Fe II and Mg II lines at the same time as the D I and H I lines. By taking advantage of the smaller thermal broadening of the heavier metal lines we could search for multiple velocity components along the short line of sight to Capella and separate the effects of thermal broadening from turbulent broadening. We discuss the measurements for Fe II and Mg II in § 3.1, and we use those results to analyze the D I and H I absorption in § 3.2.

3.1. *The Interstellar Lines of* Fe II *and* Mg II

The narrow Fe II and Mg II *h* and *k* interstellar absorption lines are superposed on broad stellar chromospheric emission lines. Interstellar line profiles were obtained by fitting fifth-order polynomials to the emission in the region of the interstellar absorption. The continuum normalized line profiles are shown in Figure 2 as plots of normalized flux versus heliocentric velocity. The measurements are shown by dots with 1 σ error bars attached. The errors were derived from the gross signal, assuming Poisson statistics.

The observed absorption lines, centered near 22 km s^{-1}, are symmetrical and show no evidence for multiple component

TABLE 2

INTERSTELLAR LINE PARAMETERS FOR Mg II AND Fe II

Parameter	Mg II *h*	Mg II *k*	Fe II 2600 Å
λ_c (Å)	2802.9175	2795.7429	2599.5752
v_c (km s^{-1})	22.75	23.04	20.68
b (km s^{-1})	2.52	2.64	2.40
N_L (cm^{-2})	6.49×10^{12}	6.44×10^{12}	3.01×10^{12}
τ_0	3.30	6.25	1.09
χ^2	2.79	9.18	1.40

TABLE 3

INTERSTELLAR LINE PARAMETERS FOR H I AND D I

PARAMETER	IF $N_H = 1.60 \times 10^{18}$		IF $N_H = 1.70 \times 10^{18}$		IF $N_H = 1.80 \times 10^{18}$ (best fit)	
	D	H	D	H	D	H
λ_c (Å)	1215.4265	1215.756	1215.4267	1215.756	1215.4269	1215.756
v_c (km s^{-1})	21.93	21.74	21.97	21.74	22.04	21.74
b (km s^{-1})	7.81	10.91	7.78	10.87	7.81	10.91
N_L (cm^{-2})	2.91×10^{13}	1.60×10^{18}	2.92×10^{13}	1.70×10^{18}	2.97×10^{13}	1.80×10^{18}
χ^2	0.856	...	0.799	...	0.897	...
$T(K)$	6985.		6928.		6992.	
ξ (km s^{-1})	1.66		1.67		1.66	
$(D/H)_{LISM}$	1.82×10^{-5}		1.72×10^{-5}		1.65×10^{-5}	

PARAMETER	IF $N_H = 1.90 \times 10^{18}$		IF $N_H = 2.00 \times 10^{18}$		IF $N_H = 2.10 \times 10^{18}$	
	D	H	D	H	D	H
λ_c (Å)	1215.4269	1215.756	1215.4269	1215.756	1215.4268	1215.756
v_c (km s^{-1})	21.98	21.74	22.03	21.74	21.98	21.74
b (km s^{-1})	7.91	10.06	7.89	11.03	8.14	11.40
N_L (cm^{-2})	2.99×10^{13}	1.90×10^{18}	3.00×10^{13}	2.00×10^{18}	3.10×10^{13}	2.10×10^{18}
χ^2	0.810	...	0.832	...	0.854	...
$T(K)$	7196.		7156.		7661.	
ξ (km s^{-1})	1.63		1.63		1.56	
$(D/H)_{LISM}$	1.57×10^{-5}		1.50×10^{-5}		1.47×10^{-5}	

structure. We conclude that the Fe II and Mg II data reveal no additional velocity components of the interstellar gas within ± 40 km s^{-1} of the main component. If multiple component structure exists, that structure must be at a scale which is unresolved by the GHRS. Note that the instrumental spread function for these observations is approximated by a Gaussian with FWHM of 3.54 km s^{-1} for the Mg II lines and 3.27 km s^{-1} for the Fe II line (see Figs. 4–10 of Duncan 1992).

To determine the column densities and absorption line centroid velocities, and to search for evidence of structure within the absorption at a scale below the width of the instrumental spread function, we fit the normalized absorption lines with Gaussian-broadened absorption lines parameterized by the standard Gaussian velocity spread parameter b (km s^{-1}) (see Spitzer 1978). For pure thermal line broadening, b (km s^{-1}) $= (2kT/m)^{1/2} = 0.129(T/A)^{1/2}$, where A is the atomic weight. For a combination of thermal line broadening and macroscopic turbulent broadening, $b^2 = (2kT/m) + \xi^2$, where the most probable speed of the turbulent mass motions represented by ξ (km s^{-1}) is assumed to be described by a Gaussian function which can be added in quadrature to the thermal Doppler broadening.

In the absorption line fitting process the free parameters are the centroid velocity v_c, the value of b, and the column density of Fe II or Mg II. The Mg II h and k lines were fitted independently. The instrumental spectral spread functions used to blur the simple trial spectrum are assumed to be described by Gaussians with the values of FWHM given in Table 1. Values for the oscillator strengths, f, and vacuum wavelengths for the three lines are taken from Morton (1991). The results of the fitting process are shown in Figure 2 and are listed in Table 2, where λ_c is the observed centroid wavelength, v_c is the velocity displacement of λ_c from the laboratory vacuum wavelength, and τ_o is the line center optical depth of the fitted profile before instrumental blurring. In the figure the solid lines show the best-fit instrumentally blurred profiles, while the dashed lines show the profiles before the instrumental blurring function was applied. The best fit is taken as that provided by the combination of column density, centroid velocity, and broadening parameter that gives the minimum value of χ^2, which is also listed in Table 2. The Mg II data have very high S/N values. The inadequacy of the Mg II profile fit is reflected in the large values of χ^2, particularly for the k line. The large values of χ^2 may partially reflect our uncertain knowledge about the true nature of the echelle mode instrumental spread function which we have simply assumed to be described by a Gaussian.

The measured heliocentric radial velocities v_c of the two Mg II lines (22.75 and 23.04 km s^{-1}) agree well with each other but differ from the velocity of the Fe II line (20.68 km s^{-1}) by approximately 2.2 km s^{-1}. This difference is only slightly larger than the 1 σ errors of 1.5 km s^{-1} we expect from our wavelength calibration.

The interstellar profile fits imply that the small-scale velocity structure of the Fe II and Mg II absorption is only approximately described by Gaussian lines with $b = 2.4$–2.6 km s^{-1}. The difference in the values of b and N_L derived for the two Mg II lines and the large values of χ^2 imply that the actual line broadening is more complex than that represented by a simple Gaussian profile. If the Fe II and Mg II lines are formed in the warm interstellar medium with $T = 7000 \pm 200$ K (the value we derive for D I in § 3.2), we would expect the thermal Doppler broadening contribution to the measured value of b to be 2.19 km s^{-1} for Mg and 1.44 km s^{-1} for Fe. In addition to thermal broadening, there apparently is macroscopic turbulence contributing at a level such that ξ is approximately given by 1.66 km s^{-1} (see § 3.2).

The column densities for Mg II and Fe II are reliably determined. For Mg II we assign greater confidence to the value of

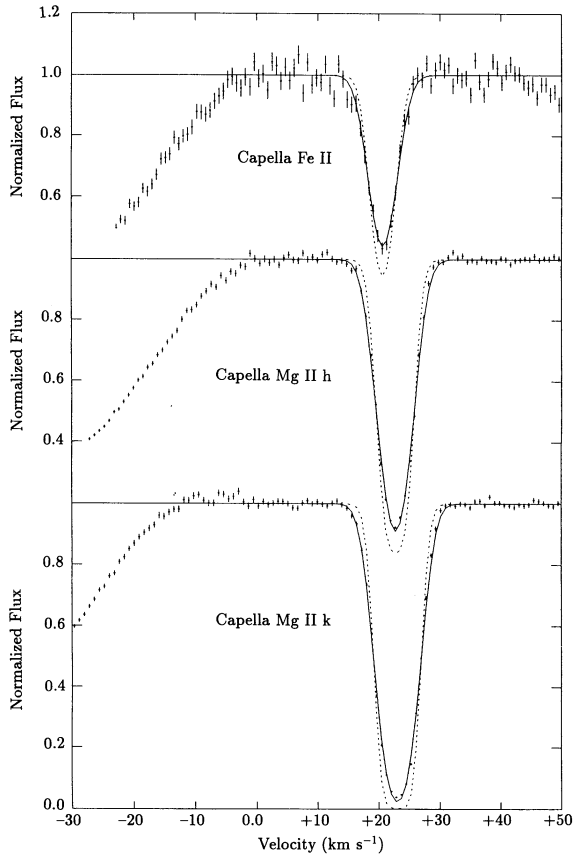

FIG. 2.—*Top*: GHRS spectrum of the Fe II 2599 Å line profile (± 1 σ error bars), the best fit to the data (*solid line*), and the best-fit profile before application of the instrumental smearing (*dashed line*). The column density is $N_{\rm Fe\,II} = 3.01 \times 10^{12}$ cm^{-2}. *Middle*: GHRS spectrum of the Mg II 2803 Å line profile (± 1 σ error bars), the best fit to the data (*solid line*), and the best-fit profile before application of the instrumental smearing (*dashed line*). The column density is $N_{\rm Mg\,II} = 6.49 \times 10^{12}$ cm^{-2}. *Bottom*: GHRS spectrum of the Mg II 2796 Å line profile (± 1 σ error bars), the best fit to the data (*solid line*), and the best-fit profile before application of the instrumental smearing (*dashed line*). The column density is $N_{\rm Mg\,II} = 6.44 \times 10^{12}$ cm^{-2}.

$N_{\rm Mg\,II}$ based on the weaker *h* line. The implications for the gas-phase abundance of Mg and Fe in the warm interstellar medium are discussed in § 4.1.

3.2. *The Interstellar Lines of* D I *and* H I

The interstellar lines of D I and H I are separated by 0.3307 Å or 81.55 km s^{-1}. The wings of the H I absorption influence the continuum for the D I absorption. Therefore, the two absorptions must be analyzed together. For our analysis we have adopted the atomic parameters including wavelengths, *f*-values, and damping constants for H I and D I as tabulated by Morton (1991). The analysis allows for the fact that both D I and H I are closely spaced doublets with $\Delta\lambda = 0.0054$ Å, which corresponds to a velocity spacing of 1.33 km s^{-1}. The stronger doublet line has twice the *f*-value of the weaker line and is situated at shorter wavelengths. The analysis also assumes that the instrumental spectroscopic spread function for the region of the H I and D I lines is well represented by a Gaussian function with FWHM = 3.57 km s^{-1}.

We developed an iterative method for obtaining $v_{\rm D\,I}$, $b_{\rm D\,I}$, $N_{\rm D\,I}$, and $N_{\rm H\,I}$ that operates as follows.

Using an approximate continuum estimate for the D I doublet, we derive values of $v_{\rm D\,I}$ and $b_{\rm D\,I}$. We assume that the D I absorption is well represented by overlapping doublet lines broadened with a simple Doppler Gaussian function defined by a single value of $b_{\rm D\,I}$. We also assume that the H I has the same velocity as the D I and a Doppler broadening function given by $b_{\rm H\,I} = (2)^{1/2} \times b_{\rm D\,I}$, where the $(2)^{1/2}$ allows for the mass difference between H and D. We then reconstruct the "H I continuum" by dividing the observed spectrum by $e^{-[N_{\rm H\,I}\sigma_{\rm H\,I}]} \otimes {\rm SF}(\Delta\lambda)$, where the value of $N_{\rm H\,I}$ is selected to give the best continuum reconstruction, $\sigma_{\rm H\,I}$ is the wavelength-dependent cross section for the H I doublet including natural broadening and Doppler broadening, and SF($\Delta\lambda$) is the instrumental blurring function, which is convolved with the exponential term. What we call here the "H I continuum" is the intrinsic Lyα emission line profile of Capella before interstellar absorption. Selection of the best-fit value of $N_{\rm H\,I}$ provides a reconstructed continuum which is used to derive new values of $v_{\rm D\,I}$ and $b_{\rm D\,I}$ by fitting a spline to define the continuum in the vicinity of the D I line. The process produces slightly different values of $v_{\rm D\,I}$ and $b_{\rm D\,I}$, which are then used to repeat the H I continuum reconstruction process until convergence is achieved.

The final iteration in the fitting process allows for a turbluence contribution to the derived value of $b_{\rm D\,I}$, which influences the input value of $b_{\rm H\,I}$. The turbulent contribution to $b_{\rm D\,I}$ and the temperature of the absorbing cloud toward Capella are estimated by performing a least-squares fit to the values of $b_{\rm D\,I}$, $b_{\rm Fe\,II}$, and $b_{\rm Mg\,II}$ with the assumption that the *b* values should behave as $b^2 = (0.129)^2 T/A + \xi^2$. This fit utilizes only the *b* value for the weaker Mg II line, since that line has approximately the same central depth as the D I line and is better fitted by the simple Gaussian profile (see Table 2). After we determine values for *T* and ξ, the final value of *b* used for the H I profile in the reconstruction process is taken to be $b_{\rm H\,I} = [(0.129)^2 T + \xi^2]^{1/2}$. Since the derived value of ξ is quite small (1.66 km s^{-1}), the inclusion of this step in the profile fitting process has an insignificant effect on the final derived value of $N_{\rm H\,I}$. As a last step in the process a value of $N_{\rm D\,I}$ is obtained from the profile fit to the D I line through a χ^2 minimization procedure. In implementing this procedure the errors in the data are assumed to be dominated by Poisson statistics. The intrinsic line center optical depth of the D I line is 2.85 ± 0.03.

Table 3 lists the interstellar parameters derived for a range of $N_{\rm H\,I}$, including the best-fit value of $N_{\rm H\,I} = 1.80 \times 10^{18}$ cm^{-2}. An illustration of the best-fit H I continuum reconstruction is found in Figure 3. The best-fit reconstruction to the H I continuum leaves a weak "apparent" absorption feature on the short-wavelength wing of the reconstructed line continuum. We have searched very carefully to try to identify the likely origin of the feature. The feature could be eliminated by a shift of approximately -1 km s^{-1} in the centroid position of the H I absorption profile with respect to the D I absorption profile. However, such a shift would imply an error of approximately 1.2% in the dispersion constants used for the wavelength calibration for the spectrum. There is no evidence that dispersion errors this large are present in carefully processed GHRS echelle mode data. However, if such an error were present, the resulting best-fit value of $N_{\rm H\,I}$ would be 1.9×10^{18} cm^{-2}, which is within the error limits that we have assigned to our results (see below). If the feature is due to an extra absorption component of H I near $v = -25$ km s^{-1}, the required column density to produce the weak depression is estimated to be $N_{\rm H\,I} = 2 \times 10^{12}$ cm^{-2}, which is 10^{-6} of the gas found in the principal absorption near $v = +22$ km s^{-1}. The column

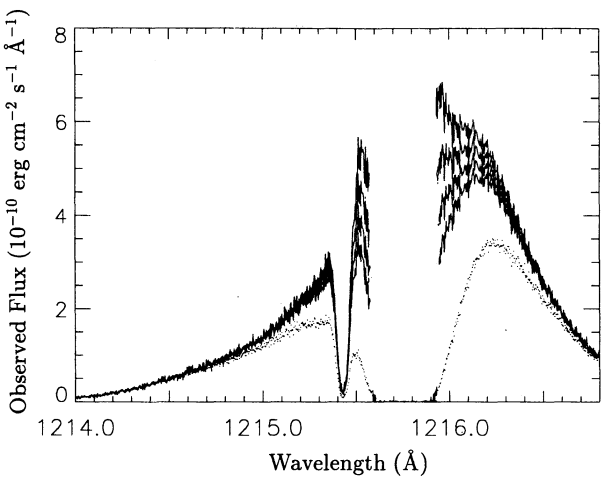

FIG. 3.—GHRS spectrum of the Lyα line (*lower profile*) and four reconstructed profiles of the intrinsic Lyα emission line of Capella obtained by dividing the observed profile by $[e^{-\tau_\lambda} \otimes \mathrm{SF}(\Delta\lambda)]$, where τ_λ is the interstellar hydrogen opacity and SF($\Delta\lambda$) is the instrumental spectral spread function. The top four curves, from top to bottom, are for $N_{\mathrm{H\,I}} = 2.20 \times 10^{18}$, $N_{\mathrm{H\,I}} = 2.00 \times 10^{18}$, $N_{\mathrm{H\,I}} = 1.80 \times 10^{18}$, and $N_{\mathrm{H\,I}} = 1.60 \times 10^{18}$, cm^{-2}.

density of this velocity component would be too small to be observed in any other line. It is also possible that the apparent shift, if real, could be due to radiative acceleration of deuterium relative by an anisotropic radiation field as suggested by Bruston et al. (1981) among others. For another possible explanation see Appendix B.

The best fit to the D I absorption line is shown in Figure 4. The solid line is the instrumentally blurred fit to the data which are shown as the dots with attached 1 σ error bars. The dashed line illustrates the input profile before instrumental blurring was applied. The GHRS almost completely resolves the D I absorption, because of its great breadth from thermal broadening. Uncertainties in determining the column density of D I will be mostly determined by continuum placement errors

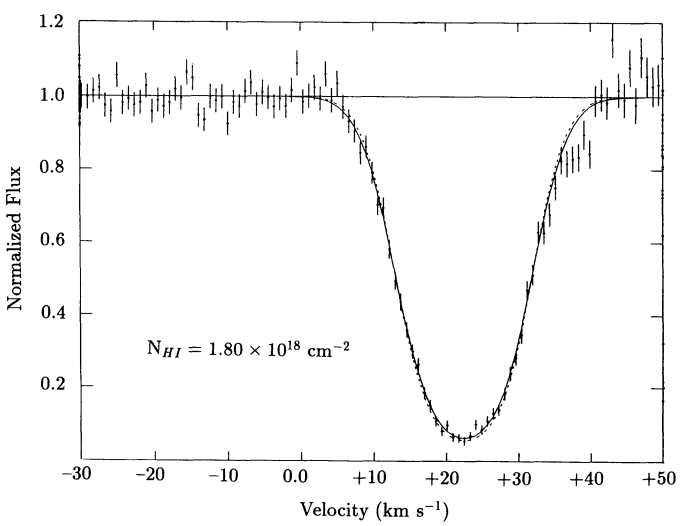

FIG. 4.—GHRS spectrum of the D I Lyα line profile (± 1 σ error bars), the best fit to the data (*solid line*), and the best-fit profile before application of the instrumental smearing (*dashed line*). The column density is $N_{\mathrm{D\,I}} = 2.97 \times 10^{13}$ cm^{-2}.

associated with the imprecision in determining the value of $N_{\mathrm{H\,I}}$.

In order to study errors in the derived parameters, we varied the value of $N_{\mathrm{H\,I}}$ until in our judgment the fit to the reconstructed continuum became unacceptable. Figure 3 shows the reconstructed results for the best fit and these upper and lower limits to $N_{\mathrm{H\,I}}$. The additional entries in Table 3 illustrate the sensitivity of the derived values of $v_{\mathrm{D\,I}}$, $N_{\mathrm{D\,I}}$, $b_{\mathrm{D\,I}}$, ξ, and T to the choice of $N_{\mathrm{H\,I}}$.

From Figures 3 and 4 and Table 3 we conclude that $N_{\mathrm{H\,I}} = 1.80(\pm 0.10) \times 10^{18}$ cm^{-2}, $N_{\mathrm{D\,I}} = 2.97 \pm 0.05 \times 10^{13}$ cm^{-2}, $T = 7000 \pm 200$ K, $\xi = 1.66 \pm 0.03$ km s^{-1}, and $(\mathrm{D/H})_{\mathrm{LISM}} = 1.65(+0.07, -0.08) \times 10^{-5}$. See § 3.4.2 for a discussion of the effects on the allowable range of $N_{\mathrm{H\,I}}$ and $(\mathrm{D/H})_{\mathrm{LISM}}$ of assuming a broader range of plausible intrinsic line profiles for the Capella stars. Allowing for the systematic errors associated with the derivation of $N_{\mathrm{H\,I}}$, our conclusion from § 3.4.2 is that $N_{\mathrm{H\,I}} = 1.8(+0.3, -0.1) \times 10^{18}$ cm^{-2}, which implies that $(\mathrm{D/H})_{\mathrm{LISM}} = 1.65(+0.07, -0.18) \times 10^{-5}$.

3.3. *Relative Flux Calibration of the Lyα Profile*

Initial inspection of the Lyα profile raised some questions about the relative flux calibration with wavelength, as the shape of the profile did not agree with published *IUE* spectra. In particular, the ratio of the red peak to blue peak flux in Figure 1 is 1.93, whereas the *IUE* profiles in Ayres, Schiffer, & Linsky (1983) show a ratio of 1.4 both at orbital phase 0.27 (nearly the same as the GHRS spectrum) and at phase 0.76 when the two stars are at opposite radial velocities. This discrepancy led us to question the preflight echelle blaze correction and to consider whether the Capella Lyα profile shape changes with time.

The first question can be answered by analyzing the low-dispersion spectrum of the 1161–1449 Å region obtained with the G140L first-order grating ~3 hr before acquiring the Lyα echelle spectrum. Since the light paths for the echelle A and G140L gratings are very different, comparison of the Lyα profiles convolved to the same spectral resolution provides a critical test of the shape of the echelle A spectrum. The G140L spectrum was obtained through the LSA, and spherical aberration of the *HST* primary mirror degrades its spectral resolution. We have corrected for this effect by deconvolving the observed G140L Lyα profile using the LUCY_GUESS routine with the telescope point-spread function derived from an FOC f/96 image at 1400 Å (image F96F140GC_M). Shore (1990) has described this method in detail. To compare the two profiles, we extended the red wing of the echelle A Lyα profile and convolved the resulting profile with Gaussians of different widths. Figure 5 shows the excellent match to the deconvolved G140L profile that occurs when the echelle profile is degraded to a resolution of 1500. This is expected since the nominal resolution of the G140L grating through the SSA is about 2500. We conclude that the echelle A blaze correction in the CALHRS software is probably accurate.

In Appendix A we compare the GHRS Lyα profiles of Capella with those obtained with the *Copernicus* satellite. In a companion paper, Ayres et al. (1992) have reanalyzed *IUE* spectra near phase 0.25 and 0.75. The long-term record of Lyα profiles in the *IUE* archives shows significant variability of the blue peak of the profile at phase 0.25, which may be instrumental or intrinsic to the star. The GHRS profile falls in the middle to lower range of the variations, while the profile shown by Ayres et al. (1983) falls in the extreme upper portion of the

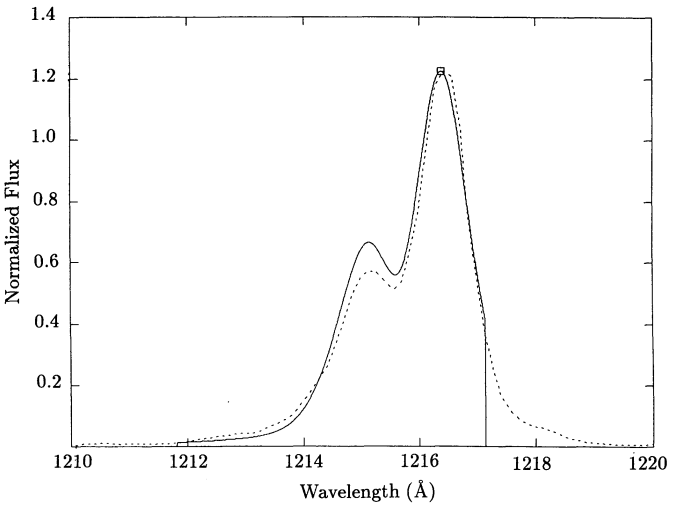

FIG. 5.—The excellent match to the deconvolved G140L Lyα profile (*dotted line*) that occurs when the echelle profile is degraded to a resolution of $\lambda/\Delta\lambda = 1500$ (*solid line*). This excellent match confirms that the relative flux calibration of the echelle data is accurate.

range, thus causing the apparent disagreement with the GHRS profile. The *Copernicus* spectra obtained near phase 0.25 also are consistent with the GHRS spectra, with red/blue peak flux ratio near 2.0 compared with the GHRS value of 1.93. Thus we are now satisfied that the relative flux calibration of the GHRS Lyα profile is accurate.

3.4. *The Intrinsic Lyα Profile of Capella*

In § 3.2 we constructed the stellar emission-line profile for the Capella system by dividing the observed spectrum by $e^{-[N_{H\,I}\,\sigma_{H\,I}]} \otimes \mathrm{SF}(\Delta\lambda)$. We now ask whether this reconstructed profile (see Fig. 3) is consistent with what we know about the Capella system and the formation of the Lyα emission line in stellar chromospheres. Since interstellar absorption removes the central portion of the Lyα line for nearly all stars except the Sun, our models of the Capella intrinsic line profile cannot be fully tested. However, a GHRS Lyα spectrum obtained near phase 0.75 would provide significant additional constraints.

Capella is a spectroscopic binary system consisting of a G8 III star (called the "G star") and a G0 III star (called the "F star") in a 104 day period orbit. At the time of the GHRS observations, phase 0.26 using the ephemeris cited by Ayres (1984, 1988), the radial velocity separation of the two stars was 53.6 km s^{-1} with the F star at negative radial velocity (displaced toward shorter wavelengths) relative to the binary system center of mass. Ayres et al. (1983) presented *IUE* spectra of the Lyα region (their Fig. 2) obtained at opposite quadratures. When these spectra and those of Ayres et al. (1992) are registered in wavelength so that the interstellar absorption features align, the stellar Lyα emission wings exhibit a positive (away from the Sun) velocity shift of 40 km s^{-1} at phase 0.76 (when the orbital velocity of the F star is also positive) compared to phase 0.27. These data can be understood with the stellar and interstellar parameters listed in Table 4.

TABLE 4

SUMMARY OF STELLAR AND INTERSTELLAR VELOCITIES

Parameter	Value	at $\phi = 0.25$	at $\phi = 0.75$	Reference
v_{com} (km s^{-1})	29.5	...	...	Batten et al. 1978
$v_{F\ star}$	...	2.0	57.0	Batten et al. 1978
$v_{G\ star}$		55.6	3.4	Batten et al. 1978
v_{LISM}	20 ± 1	...	...	Ayres 1988
$v_{F\ star} - v_{LISM}$		−20	35	
$v_{G\ star} - v_{LISM}$		34	−19	

The observed 40 km s^{-1} shift of the emission wing centroid, in phase with the 55 km s^{-1} F star orbital motion and nearly equal to it in amplitude, indicates that most of the emission in the line wings (and perhaps in the core as well) is due to the F star. Ayres et al. (1963) and Ayres (1988) have previously found that the F star contributes most of the flux for the chromospheric and transition region lines of the Capella system. The line asymmetry is the same (red peak brighter than the blue peak) at both quadratures, even though $v_{F\ star}-v_{LISM}$ changes sign from one quadrature to the next. This cannot be explained by the interstellar deuterium line absorption or the +9.5 km s^{-1} radial velocity of the center of mass of the Capella system (v_{com}) relative to the interstellar flow (v_{LISM}). This persistent asymmetry requires that either the F star, the G star, or both, have brighter red peak emission than blue peak emission. Since the F star dominates the combined profile, we model the F star profile as asymmetric.

3.4.1. *Scaled Solar Lyα Line Profiles*

We have developed a model for the intrinsic Lyα emission line from the Capella stars using the solar profile as a template. Although the Capella stars are evolved giants, rather than dwarf stars like the Sun, all three are of G spectral type and presumably have chromospheres with active regions, so that the solar Lyα profile may provide a qualitative guide for the Capella stars. In particular, the quiescent Sun profile (taken from Vidal-Madjar 1977) has steep wings and emission features near line center of about equal intensity with a pronounced central reversal about 30% deep and 0.4 Å wide (see Fig. 7). This self-reversal is produced by the high scattering albedo of the Lyα line in the solar chromosphere. Because the electron densities in the chromospheres of the Capella giants are probably an order of magnitude lower than those in the Sun, the larger scattering albedos imply that the central reversals are at least as deep for the Capella giants, although the central absorption features may be partially filled in by turbulent velocity gradients or inhomogeneous structures. The rapid rotation of the F star ($v \sin i = 53$ km s^{-1}) will also partially fill in the self-reversal feature for this star.

Since the Lyα spectrum of Capella clearly shows broader wings than the Sun (due to the increased column thickness of giant chromospheres, expected from the chromospheric scaling laws of Ayres 1979), we apply a nonlinear rescaling of the wavelength variable of the solar profile to broaden the wings. This is accomplished by replacing $\Delta\lambda(=\lambda - \lambda_c)$ by $\Delta\lambda \times (\Delta\lambda/\delta)^y$, where y is 0.3 for the G star and 0.6 for the F star, and δ is a parameter that allows the separation of the peaks to be wider for the giant stars as expected from, e.g., Basri (1980) and Gayley (1992a). A power-law wavelength rescaling is an arbitrary choice, but it does correspond to the assumption that the Lyα Planck function decreases logarithmically with depth, yielding an approximate power-law wing profile (Gayley 1992b) that will differ from star to star. For example, the solar wings are roughly proportional to $(\Delta\lambda)^{-3}$, but the profile of the F star is considerably less steep, possibly due to enhanced heating in this thicker giant chromosphere. The profile of the F star is then rotationally broadened ($v \sin i = 53$ km s^{-1}), assuming no limb darkening.

To fit the shape of the bright emission peak on the blue side of the reconstructed line profile, we found it necessary (see § 3.4) to make the F star profile asymmetric, with the red peak brighter than the blue peak. We therefore added a broad (roughly 1 Å wide) Gaussian emission component to the red peak of the F star, although we could alternatively have subtracted a broad Gaussian from the blue peak. This asymmetry not only produced good agreement with the reconstructed profile for phase 0.26, but also was needed to match the intrinsic profile at phase 0.75 based on the *IUE* profiles at this phase (Ayres et al. 1992). We found that it was not necessary to also allow the G star profile to be asymmetric.

Working with these constraints, we searched for the intrinsic stellar line profiles that would provide the best fit to the reconstructed GHRS Lyα line profile, over a range of assumed values for the interstellar hydrogen absorption. We found that only a narrow range of $N_{\rm H\,I}$ produced reconstructed profile shapes consistent with our expectations for the intrinsic line profiles. Including slightly too much interstellar opacity produced unphysical emission spikes in the inferred intrinsic profile on either side of the saturated absorption core. Including slightly too little opacity yielded inferred intrinsic profiles with a pronounced central reversal, which is implausible since an emission peak of each star falls in the self-reversed core of the other star, and the rotational smoothing of the F star partially fills in its intrinsic self-reversal.

Figure 6 shows the reconstructed line profiles for $N_{\rm H\,I} = 1.6$, 1.8, and 2.0×10^{18} cm^{-2} and our best-fit models for the intrinsic line profile from the Capella system. Also shown are the intrinsic profiles for the individual stars. The intrinsic line profiles were also chosen to be roughly consistent with the *IUE* profiles at the opposite quadrature, phase 0.75, which provides a powerful additional constraint and is an essential step in removing the ambiguity in the decomposition. As mentioned above, an important property of all of the model profiles we considered is that the red peak of the F star lies near the core of the G star, so that the sum of the profiles can show only a weak self-reversal. We believe that this is a critical constraint on plausible values of $N_{\rm H\,I}$. From Figure 6 and similar calculations at intermediate values of $N_{\rm H\,I}$, the inferred intrinsic profiles that meet this constraint lie in the range $N_{\rm H\,I} = 1.7$–1.9×10^{18} cm^{-2}. A χ^2 test of the difference between the observed profile from the edges of the saturated core to the emission peaks and the sum of the intrinsic profiles folded through the interstellar medium (shown in Fig. 6*a*) show a minimum near $N_{\rm H\,I} = 1.7 \times 10^{18}$ cm^{-2}. Thus our analysis of the Lyα profiles at both quadratures, under the assumption that the intrinsic stellar profiles can be reasonably approximated by scaled solar profiles, leads to an uncertainty of $\pm 0.1 \times 10^{18}$ cm^{-2} in $N_{\rm H\,I}$. We will characterize this as a random error, corresponding to ±6%.

3.4.2. *Comparison with the Lyα Profile of δ Lep and Systematic Errors in $N_{\rm H\,I}$*

After completing the analysis of the interstellar hydrogen absorption just described, it was brought to our attention that some important information is already known about the intrinsic Lyα profile for a star with the same spectral type as the Capella G star. The star δ Lep (=HD 39364) is a 4th mag G8 III or K0 III star with a radial velocity 99.3 km s^{-1}. In their high-dispersion *IUE* spectrum of δ Lep, Neff et al. (1990) detected the red emission peak and the red wing of this star only partially absorbed by interstellar hydrogen due to its high radial velocity. They reconstructed the whole Lyα profile by correcting for the uncertain interstellar absorption and assuming that the intrinsic profile is symmetric.

Figure 7 compares this profile smoothed to the instrumental resolution of *IUE* with the solar profile of Vidal-Madjar (1977) and the intrinsic profiles of the Capella F and G stars for the case of $N_{\rm H\,I} = 1.8 \times 10^{18}$ cm^{-2}. The vertical scale of each profile is arbitrarily chosen to allow comparison of the overall shapes. The intrinsic profile of δ Lep is very similar to our assumed profile for the Capella G star with a peak separation of 0.58 Å compared with 0.50 Å for the G star, a FWHM of 1.03 Å compared with 1.07 Å for the G star, and a central reversal depth of 50% compared with 53% for the G star. This is strong evidence for the accuracy of our scaling procedure. We cannot test the shape of the F star by comparison with δ Lep, but the central reversal of the F star must be reduced by rapid rotation.

Although δ Lep has the same spectral type as the Capella G star, it is probably an older and less active star as indicated by its high space velocity, low metallicity, and surface flux of the C IV 1550 Å emission line which is several times smaller than that of the Capella G star. This implies that the Capella G star has a larger heating rate in its transition region and chromosphere which could fill in the central reversal of the Lyα line. We do not know the extent of this filling-in, but the profile of the Lyα line in solar plages (see Basri et al. 1979) has a flat top. Figure 8 shows that $N_{\rm H\,I}$ could be as large as 2.1×10^{18} cm^{-2} and still be consistent with the observed line shape at phase 0.25. Since flat-topped intrinsic line profiles predict the largest value of $N_{\rm H\,I}$, we therefore extend the range of plausible values of $N_{\rm H\,I}$ to $1.8(+0.3, -0.1) \times 10^{18}$ cm^{-2}. The range in $({\rm D/H})_{\rm LISM}$ then becomes $1.65(+0.07, -0.18) \times 10^{-5}$. We keep the values of $T = 7000 \pm 200$ K and $\xi = 1.66 \pm 0.03$ km s^{-1} since the profile width parameters at the largest value of $N_{\rm H\,I}$ may not be accurate.

In a companion paper, Ayres et al. (1992) fit the lower resolution Capella profiles obtained by *IUE* at both quadratures using purely empirical profiles without scaling from the Sun. The best-fit G star profiles have little or no self-reversal, from which they derive $N_{\rm H\,I} = 2.0(\pm 0.2) \times 10^{18}$ cm^{-2}, which satisfactorily overlaps our result.

3.4.3. *Intrinsic Lyα Luminosities for the Capella Stars*

Table 5 summarizes the Lyα line surface fluxes $F_{\rm Ly\alpha}$, luminosities $L_{\rm Ly\alpha}$, and ratios of $L_{\rm Ly\alpha}$ to the bolometric luminosity $L_{\rm bol}$ for the Capella G and F stars with no interstellar absorption and for the adopted range in $N_{\rm H\,I}$. We have assumed a distance of 12.5 pc, stellar radii of 8.8×10^{11} cm and 6.1×10^{11} cm, and bolometric luminosities of 3.2×10^{35} ergs s^{-1} and 2.8×10^{35} ergs s^{-1} for the G and F stars, respectively

TABLE 5

INTRINSIC Lyα LUMINOSITIES FOR THE CAPELLA STARS

$N_{\rm H\,I}$ (10^{18} cm^{-2})	$F_{\rm Ly\alpha}$ (10^5 ergs cm^{-2} s^{-1})		$L_{\rm Ly\alpha}$ (10^{28} ergs s^{-1})		$L_{\rm Ly\alpha}/L_{\rm bol}$ (10^{-6})	
	G Star	F Star	G star	F Star	G Star	F Star
1.7	4.4	15	430	760	13	27
1.8	5.0	15	490	760	15	27
2.1	5.5	15	540	760	17	27
Sun	1.8		1.1		3.0	

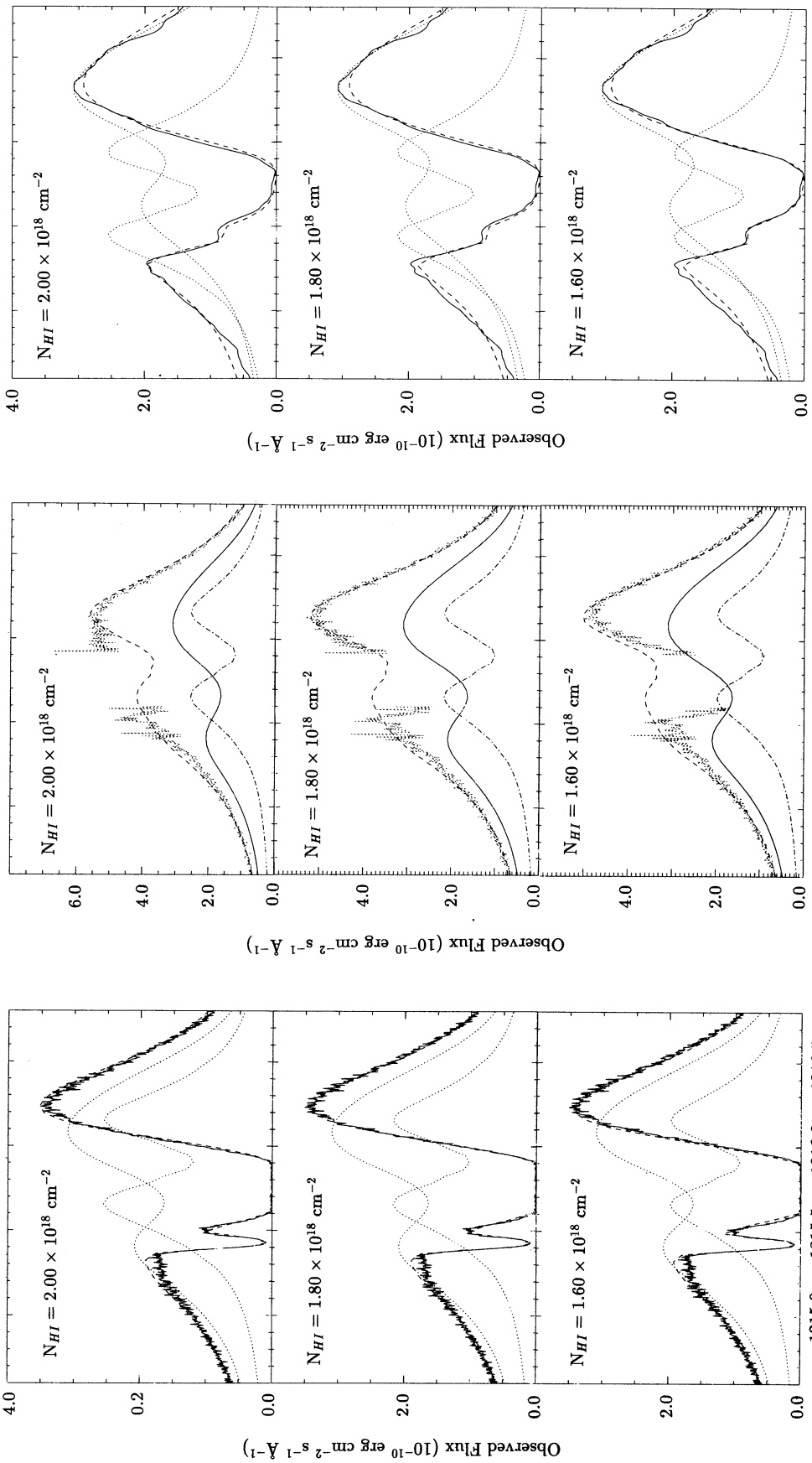

FIG. 6a

FIG. 6b

FIG. 6c

FIG. 6.—(*a*) Observed GHRS spectrum (*solid line*), the intrinsic Lyα emission lines of the Capella F and G stars (*dotted lines*), and the sum of these intrinsic stellar lines folded through the interstellar medium (*dashed line*). The top panel is for $N_H = 2.0 \times 10^{18}$ cm^{-2}, the middle panel is for $N_{H\,I} = 1.8 \times 10^{18}$ cm^{-2}, and the lower panel is for $N_{H\,I} = 1.6 \times 10^{18}$ cm^{-2}. A value of $N_{D\,I} = 2.97 \times 10^{13}$ cm^{-2} was used in these calculations. (*b*) The reconstructed composite stellar emission line (*dotted line*) obtained by dividing the observed GHRS spectrum by the interstellar D I and H I absorption, the intrinsic Lyα emission lines of the Capella F (*solid line*) and G stars (*dashed-dot line*), and the sum of these intrinsic stellar lines (*dashed line*). The top panel is for $N_{H\,I} = 2.0 \times 10^{18}$ cm^{-2}, the middle panel is for $N_{H\,I} = 1.8 \times 10^{18}$ cm^{-2}, and the lower panel is for $N_{H\,I} = 1.6 \times 10^{18}$ cm^{-2}. A value of $N_{D\,I} = 2.97 \times 10^{13}$ cm^{-2} was used in these calculations. (*c*) The observed *IUE* spectrum at phase 0.75 (*solid line*), the intrinsic Lyα emission lines of the Capella F and G stars (*dotted lines*), and the sum of these intrinsic stellar lines folded through the interstellar medium (*dashed line*). The top panel is for $N_{H\,I} = 2.0 \times 10^{18}$ cm^{-2}, the middle panel is for $N_{H\,I} = 1.8 \times 10^{18}$ cm^{-2}, and the lower panel is for $N_{H\,I} = 1.6 \times 10^{18}$ cm^{-2}. A value of $N_{D\,I} = 2.97 \times 10^{13}$ cm^{-2} was used in these calculations.

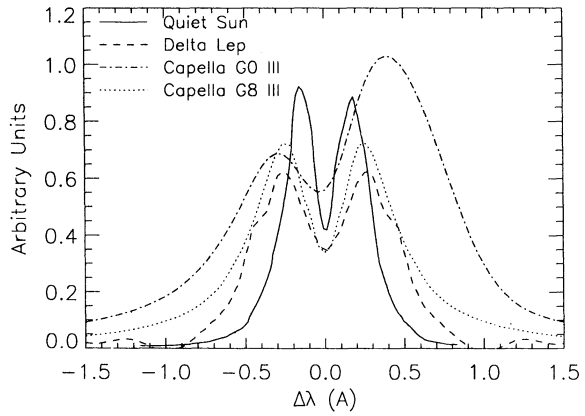

FIG. 7.—Comparison of the intrinsic Lyα profiles of the Sun (Vidal-Madjar 1977), δ Lep (Neff et al. 1990), and the F and G stars of Capella for the model for $N_{HI} = 1.8 \times 10^{18}$ cm^{-2}. The profiles are plotted in the rest frames of each star.

(Batten, Hill, & Lu 1991). Mean quiet Sun quantities are included for comparison. We note that all three measures of the Lyα emission are larger for the F star than for the G star, but both Capella stars are brighter than the Sun in Lyα. We find that the F star has about 1.6 times the luminosity of the G star in Lyα. This may be compared with the ratio of about 3 for low-excitation lines like O I, Si II, and Mg II and the ratio of 10 for the C IV line found by Ayres (1988).

4. DISCUSSION

4.1. *Gas-Phase Abundances in the Warm Cloud toward Capella*

The measurements of the interstellar lines of Fe II and Mg II provide an estimate of the gas-phase abundances of Fe and Mg in the warm cloud in the direction of Capella. Since the ionization potentials of Fe and Mg are Fe I (7.87 eV), Fe II (16.18 eV), Mg I (7.74 eV), and Mg II (15.03 eV), Fe II and Mg II should be the dominant ionization states of Fe and Mg in diffuse neutral hydrogen clouds. However, some Fe II and Mg II may exist in regions of ionized hydrogen and the total column densities we measure for Fe II and Mg II may include contributions from ionized gas in the local ISM. From Tables 2 and 3, we find that N(H I) = 1.80 × 10^{18}, N(Fe II) = 3.01 × 10^{12}, and N(Mg II) = 6.49 × 10^{12} cm^{-2}, respectively. Therefore, log [N(Fe II)/N(H I)] = −5.77 and log [N(Mg II)/N(H I) = −5.44. Comparing these numbers to the solar abundances of Fe and Mg, log [Fe/H]$_\odot$ = −4.49 and log [Mg/H]$_\odot$ = −4.41 from Anders & Grevesse (1989), and assuming that the contributions to Fe II and Mg II from ionized gas are negligible, we derive the logarithmic depletions, D(Fe) = [N(Fe II)/N(H I)] − log [Fe/H]$_\odot$ = −1.28 and D(Mg) = [N(Mg II)/N(H I)] − log [Mg/H]$_\odot$ = −1.03 in the warm gas toward Capella.

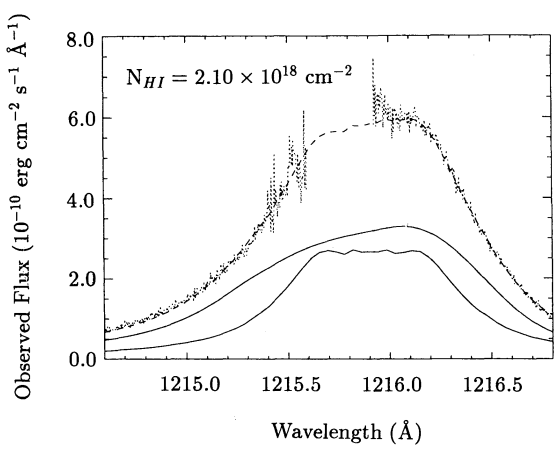

FIG. 8.—The reconstructed composite stellar emission line obtained by dividing the observed GHRS spectrum by the interstellar absorption (*dotted line*), the intrinsic Lyα emission lines of the Capella F and G stars assumed to have flat tops (*solid lines*), and the sum of these intrinsic stellar lines (*dashed line*). This calculation is for $N_{HI} = 2.1 \times 10^{18}$ cm^{-2} and $N_{DI} = 2.97 \times 10^{13}$ cm^{-2}.

These depletion values can be compared to the *Copernicus* satellite estimates of depletion in the warm interstellar medium from Jenkins, Savage, & Spitzer (1986) of D_w(Fe) = −1.4 and D_w(Mg) = −0.3. The value for Fe is similar to that measured for the Capella sight line, while the value for Mg differs by 0.7 dex. Some of this difference may be due to a systematic error in the f-values for the far-ultraviolet Mg II lines near 1240 Å used in the *Copernicus* study. Cardelli et al. (1991a) noted in an analysis of GHRS echelle mode data for interstellar gas toward ξ Per that the far-UV lines of Mg II yielded Mg II column densities 0.46 dex larger than obtained from an analysis of the very strong but damped Mg II lines near 2800 Å. Although there is a difficulty with the Mg II results, the measurements for Fe II clearly reveal that substantial gas-phase depletion occurs in the cloud toward Capella. Evidently the Fe in the cloud in the direction of Capella is mostly found in interstellar dust. In their extensive survey of 223 stars in the Galaxy, Van Steenberg & Shull (1988) find an even larger mean depletion D_w(Fe) = −1.97, with the value for the Capella line of sight near the lower end of the distribution.

4.2. *The Temperature and Flow Velocity in the Warm LISM*

The kinetic temperature of the warm neutral gas in the cloud in the direction of Capella is accurately determined from the high-quality D I line profile fit shown in Figure 4. The resulting value, T = 7000 ± 200 K, includes a correction for a modest amount of macroscopic turbulent broadening estimated from the measurements for Fe II and Mg II (see § 3.1). Previous measures of temperature in the warm, neutral ISM have been reviewed by Kulkarni & Heiles (1987), who cite a rough estimate of $T \sim 8000$ K.

The 21 cm emission-absorption comparison technique has provided many lower limits to the temperature in the warm medium but very few actual measurements, because cold clouds along the line of sight can bias the inferred temperature. Occasionally it is possible to measure the small absorption optical depths toward very bright radio continuum sources associated with the warm medium and to determine a temperature. The highest measured temperature from the radio technique is ~6000 K in the warm medium towards Cygnus A (Kalberla, Mebold, & Reich 1980). A few additional temperature estimates have come from profile fits and curve of growth techniques applied to *Copernicus* satellite 13 km s^{-1} resolution data for UV lines toward several hot stars situated in the LISM (see York & Frisch 1984). For example, Gry et al. (1985) inferred T = 11,000–12,500 K for the line of sight toward β CMa from their analysis of the Lyman lines, but this result would be too large if unresolved velocity components are present. Also, analysis of solar Lyα and He I 584 Å radiation backscattered from the LISM gas flowing into the solar system yields estimates of T = 8000 ± 1000 K (Bertaux et al.

TABLE 6

SUMMARY OF LOCAL INTERSTELLAR MEDIUM PROPERTIES

Star	l	b	d (pc)	$H_{\rm H\,I}$ (10^{17} cm^{-2})	$b_{\rm H\,I}$ (km s^{-1})	$n_{\rm H\,I}$ (cm^{-3})	D/H (10^{-5})	Reference
α Cen A	316°	−1°	1.3	6–10	~8–10	0.15–0.25	0.17–0.36	1
				2.4–12	10–16	0.06–0.30	0.9–2.0	2
				1–8	≥11	0.03–0.21	≥0.81	3
α Cen B	316°	−1°	1.3	≤6	≥14	≤0.15	≥1.5	3
ε Eri	196°	−48°	3.3	10–16	6–14	0.10–0.16	1.1–2.9	2
				2–28	3–17	0.01–0.27	≥0.6	3
ε Ind	336°	−48°	3.4	~10	~11	~0.1	~1.8	2
Procyon	214°	13°	3.5	10–14	10–15	0.09–0.13	0.7–1.9	4
				10–22	3–15	0.09–0.20	≥ 0.8	3
Capella	163°	5°	12.5	9–15	10	0.02–0.04	2.2–9.6	1
				15–19	8–10	0.04–0.05	1.8–4.0	2
				9–17	3–12	0.022–0.04	≥2.0	5
				9–19	13–17	0.021–0.046	2.3–8.2	6
				17–21	10.9	0.044–0.055	1.47–1.72	7
λ And	110°	−15°	24	20–60	10–12	0.03–0.08	0.13–0.50	8
				4–24	14–22	0.006–0.033	≥1.7	6
HR 1099	185°	−41°	33	3–7	14.6	0.003–0.007	1.2–4.5	9
				9–16	≤13	0.009–0.016	≥0.09	3

REFERENCES.—(1) Dupree, Baliunas, & Shipman 1977; (2) McClintock et al. 1978; (3) Murthy et al. 1987; (4) Anderson et al. 1978; (5) Anderson 1979; (6) Murthy et al. 1990; (7) this paper; (8) Baliunas & Dupree 1979; (9) Anderson & Weiler 1978.

1985) and $T = 7000 \pm 2000$ K (Chassefiere, Dalaudier, & Bertaux 1988).

None of these measures, however, produces the level of confidence in the temperature estimate as that provided by the D I line Doppler-broadened profile fit shown in Figure 4. In fact, the quality of the profile fit for such a short path through the LISM provides confirmation of the theoretical expectation (Spitzer 1978, Chap. 2) that a simple Maxwell-Boltzmann velocity distribution function is indeed a valid description for the particle motions in the warm, neutral interstellar medium. The agreement between our measured temperature for the warm gas in the Capella line of sight and the temperature of the gas flowing into the solar system is very gratifying.

The five interstellar lines observed with the echelle show a mean heliocentric velocity $v_{\rm LISM} = 22.0 \pm 0.9$ km s^{-1}. This may be compared with the expected 1 σ error of 1.5 km s^{-1} associated with the wavelength calibration of the Capella echelle mode data. Our value of $v_{\rm LISM}$ is consistent with the value of 20 ± 1 km s^{-1} determined by Ayres (1988) using *IUE* spectra that were calibrated using the known γ-velocity of the Capella system (Batten, Fletcher, & Mann 1978). Crutcher (1982) derived the mean flow vector for the LISM from measurements of Na I absorption toward stars within 100 pc assuming that the flow is coherent. This flow vector predicts that the velocity along the Capella line of sight should be 20.0 km s^{-1}. Thus we find no inconsistency between the observed flow velocity for the Capella line of sight and the mean flow in the LISM.

4.3. *Comparison with Previous Measurements of* D/H *toward Nearby Stars*

The critical role that the primordial value of D/H plays in understanding the evolution of the universe has stimulated observers to measure this quantity in a variety of environments using a variety of spectroscopic techniques. Some recent reviews of this topic include those of Laurent (1983), Boesgaard & Steigman (1985), Pasachoff & Vidal-Madjar (1989), and Pagel 1990). The interstellar hydrogen and deuterium absorption features have been studied using both *Copernicus* and *IUE* spectra, which have resolutions of $\lambda/\Delta\gamma \approx 20{,}000$ and 10,000, respectively. Table 6 summarizes the results of these studies using Capella and other nearby cool stars. Studies of the D/H ratio and physical properties of the LISM within about 40 pc are feasible only using late-type stars for background sources, since O-type nondegenerate stars are more distant and hot white dwarf stars are either too faint or have deep stellar Lyα absorption features.

The large range in the inferred values of $N_{\rm H\,I}$, $n_{\rm H\,I}$, D/H, and even $b_{\rm H\,I}$ for these stars and the large cited uncertainties in these quantities indicate that the low signal/noise and inadequate spectral resolution of the *IUE* and *Copernicus* data severely limit their utility for inferring the local D/H ratio. Our derived LISM parameters for the line of sight toward Capella lie outside the error bars of many of the previous measurements, despite this short line of sight having only one velocity component. Observations for the lines of sight toward the other seven late-type stars in Table 6 do not provide sufficiently constrained values of D/H for meaningful comparison with our Capella value or to determine whether the D/H ratio is uniform within 40 pc of the Sun.

Copernicus was able to detect deuterium absorption features in the more distant OB stars as far as 1 kpc from the Sun using the Lyβ line and higher members of the Lyman series. For example, Rogerson & York (1973) inferred a value of D/H = $1.4(\pm 0.2) \times 10^{-5}$ for the 63 pc line of sight toward the B1 III star β Cen. Subsequent studies of the deuterium Lyman line features toward ϵ Persei (B0.5 III) and five other OB stars revealed transient changes in the line profiles with time scales of 2–10 hr (e.g., Gry, Laurent, & Vidal-Madjar 1983; Gry, Lamers, & Vidal-Madjar 1984). These variations are now interpreted as due to nonspherically symmetric ejections of matter, often called "puffs," that provide extra hydrogen opacity at the wavelengths of the deuterium lines. Since this

effect increases the uncertainty of the inferred D/H ratios toward the OB stars, the use of late-type stars like Capella as background sources is critical to our understanding of the D/H ratio in the LISM.

4.4. *Does the D/H Ratio Depend on Line of Sight in the LISM?*

The first analysis of *Copernicus* Lyα spectra for the lines of sight toward α Cen A and Capella (Dupree, Baliunas, & Shipman 1977) resulted in D/H ratios that differed by a factor of 16, despite the short distance to these stars. This large difference and subsequent D/H measurements that also showed large differences along different lines of sight led many authors to conclude that the D/H ratio is far from constant in the LISM. Vidal-Madjar et al. (1978) and Bruston et al (1981) considered a number of possible physical processes that could segregate deuterium from hydrogen in the LISM. They concluded that selective radiation pressure (the deuterium lines see a brighter radiation field than the more opaque hydrogen Lyman lines) and chemical fractionation could be important processes.

Our accurate measurement of D/H for the Capella line of sight suggests that the variations in D/H in the LISM provided by the earlier work may be due to errors of measurement rather than to intrinsic variations. We have come to this conclusion for the following reasons.

1. The previous D/H measurements for the Capella line of sight based on *Copernicus* and *IUE* data all lie outside the range of the present result. Since the GHRS spectra have much higher signal/noise than the previous data and for the first time spectrally resolve the lines, we conclude that the inadequate quality of the previous data is responsible for errors in D/H of a factor of 2–4, even for the star with the highest signal/noise spectrum.

2. The Lyα profiles for the other seven nearby stars in Table 6 all have lower signal/noise than the Capella profiles obtained by both *Copernicus* and *IUE* and thus are expected to have even larger errors in the D/H ratio. The data for these stars are indeed more widely scattered than those for Capella, but our value of $(D/H)_{LISM} = 1.65(+0.07, -0.18) \times 10^{-5}$ lies near the mean of the D/H ratios for the other stars. This would be consistent with a constant value of $(D/H)_{LISM}$.

3. McCullough (1992) has reanalyzed all of the *IUE* and *Copernicus* observations of interstellar Lyman line absorption toward both cool and hot stars without evidence for "puffs." He finds that all of these data are consistent with the hypothesis that D/H is constant and has the value $1.5(\pm 0.2) \times 10^{-5}$. This is an important result, since the mean value of D/H derived from the *Copernicus* data is consistent with our more precise value for the Capella line of sight. GHRS spectra of additional stars should be able to test the hypothesis of a constant value of D/H and to refine its value. Until such spectra demonstrate otherwise, our working hypothesis is that the D/H ratio in the disk of the Galaxy out to 1 kpc is uniform and has the same D/H ratio as Capella (see Fig. 9). The disk thus appears to be well mixed, presumably by supernovae explosions and stellar winds. Would it not be strange for the very local region of space to be inhomogeneous while the surrounding Galactic disk is well mixed?

We conclude that the best working hypothesis is that the D/H ratio is constant in the LISM and that the scatter in the previous results was caused by random and systematic measurement errors due to low signal-to-noise data and inadequate spectral resolution. Observations for other lines of sight

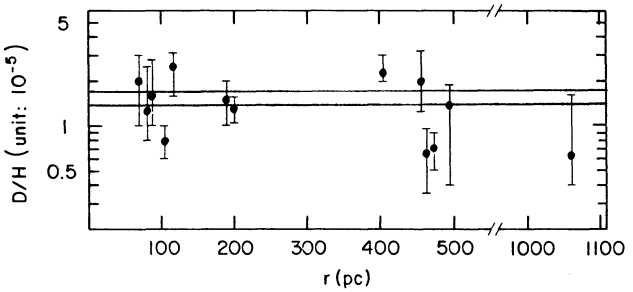

FIG. 9.—The D/H ratios for the stars observed by *Copernicus* and our value of $(D/M)_{LISM}$ shown as horizontal lines. The *Copernicus* data are from Boesgaard & Steigman (1985).

are clearly needed to verify or refute this hypothesis, to settle speculations concerning whether chemical segregation processes operate in the interstellar medium, and to set tight constraints on chemical evolution models for the Galaxy.

4.5. *Comparison with Other Measurements of* D/H *and* $N_{H\,I}$

4.5.1. *Observations of the Deuterium* 92 cm *Line*

Several groups have tried valiantly to measure the very weak 327 MHz (92 cm) ground-state hyperfine transition of atomic deuterium for comparison with the easily measured 21 cm line of atomic hydrogen. Boesgaard & Steigman (1985; Lubowich, Anantharamaiah, & Pasachoff 1989) have summarized this work. This measurement could be simply interpreted, because the resulting D/H ratio would not be subject to the uncertainties associated with studying deuterated molecules or curve-of-growth effects in optically thick aborption lines over complex lines of sight. The most recent work is that of McCullough, Heiles, & Glassgold (1991) who reported a tentative detection of the deuterium line in absorption for the 3 kpc line of sight toward Cas A. Their preliminary estimate of $D/H = 1.5 \times 10^{-5}$ was presumably affected by radio-frequency interference, because their subsequent observations with greater sensitivity have not confirmed the original result (P. R. McCullough, private communication).

4.5.2. D/H *in the Solar System*

The D/H ratios in the atmospheres of Jupiter and Saturn are similar to or perhaps slightly larger than the D/H ratio in the LISM. For example, Encrenaz & Combes (1983) from their analysis of the HD and H_2 spectra found that D/H in the atmosphere of Jupiter lies in the range $1.2–3.1 \times 10^{-5}$. Hubbard & MacFarlane (1980) and others have argued that the D/H ratio in the giant planets should be close to the presolar value. On the other hand, the D/H ratio in terrestrial seawater is 1.6×10^{-4}, about 10 times the LISM value, and similar enhancements are found in chondritic meteorites. Geiss & Reeves (1981) and Boesgaard & Steigman (1985) conclude that the D/H ratios measured in the inner solar system are larger than the LISM value because chemical fractionation at the low temperatures in the cool protosolar nebula favors the formation of deuterated molecules. An important argument for this explanation is that the D/H ratios measured from deuterated molecules in dark interstellar clouds, which are much colder than the protosolar nebula, are $10^2–10^3$ times larger than in the LISM.

4.5.3. *EUV Opacity and the Value of* $N_{H\,I}$ *toward Capella*

The HUT instrument on Astro 1 did not detect emission from Capella below 912 Å (Henry et al. 1991). This is consistent

with our derived hydrogen column density toward Capella, $N_{\rm H\,I} = 1.8 \times 10^{18}$ cm^{-2}, which requires that the interstellar hydrogen and neutral helium opacity is $\tau_\lambda = 4.0$ at 450 Å (Cruddace et al. 1974). The nondetection of Capella at $\lambda \geq$ 450 Å where the HUT spectrometer is sensitive can thus be explained by interstellar absorption. With a rocket spectrometer experiment Bobroff, Nousek, & Garmire (1984) did not detect He II 304 Å emission from Capella with a 2 σ upper limit of 0.6 photons cm^{-2} s^{-1}. This appeared to be inconsistent with their estimated intrinsic stellar emission of 2.8 photons cm^{-2} s^{-1} when they assumed a hydrogen column density of $N_{\rm H\,I} = 1.2 \times 10^{18}$ cm^{-2}, corresponding to an optical depth of 0.8 and a predicted count rate of 1.2 photons cm^{-2} s^{-1}. This apparent discrepancy goes away when we take our hydrogen column density of $N_{\rm H\,I} = 1.8 \times 10^{18}$ cm^{-2}, corresponding to an optical depth of 1.26 and a predicted count rate of 0.8 photons cm^{-2} s^{-1}.

4.6. *What Is the Primordial* D/H *Ratio?*

The value of D/H in the local region of our Galaxy, $(\rm D/H)_{LISM}$, should be a hard lower limit to the primordial value, $(\rm D/H)_p$, since deuterium is readily destroyed by nuclear reactions in stars (a process called "astration") but is not easily created in stars or in the interstellar medium. Clayton (1985) estimates that $(\rm D/H)_p \geq 3(\rm D/H)_{LISM}$ on the basis of a calculation in which he assumes that the gas in the primitive galaxy had a primordial abundance. He included star formation, astration, the return of deuterium-depleted gas to the interstellar medium as stars die, and the infall of gas with $(\rm D/H)_p$ from the Galactic halo to the disk. This result is relatively insensitive to the Galactic age, but it does depend on the rate of return of gas to the interstellar medium as stars die. The value will be greater than 3 if the infalling material is itself deuterium-poor due to astration in Galactic halo stars. The degree to which the infalling gas is depleted in deuterium is uncertain. Delbourgo-Salvador, Audouze, & Vidal-Madjar (1987) conclude that $(\rm D/H)_p$ could be much larger than 3 times $(\rm D/H)_{LISM}$. More recently Steigman & Tosi (1992) have made similar calculations resulting in a value for the survival fraction of deuterium at the present time in the range 1.5–3.0 with the larger value for models with no infalling gas. In what follows we assume this range for the survival fraction, which implies that $(\rm D/H)_p = (2.2\text{–}5.2) \times 10^{-5}$.

Some insight into the relation between $(\rm D/H)_{LISM}$ and $(\rm D/H)_p$ can be obtained by considering the related problem of the chemical history of the Galaxy, which includes the same physical processes, except that metallicity is increased by astration. Many authors have made these calculations which may be checked by the observed metallicity of disk and halo stars of different ages. In one such calculation Shore, Ferrini, & Palla (1987) find that the feedback between the infall rate and halo star formation leads to a situation in which the infall rate and its time variation can be changed by large factors and still be consistent with the stellar metallicity data. They conclude that "The system is surprisingly insensitive to tampering with the parameters." This gives us confidence that $(\rm D/H)_p = (1.5\text{–}3.0) \times (\rm D/H)_{LISM}$ is a valid assumption.

4.7. D/H *and the Evolution of the Universe*

A good estimate of $(\rm D/H)_p$ is important, because according to big bang nucleosynthesis models the light elements were created in the first 1000 s of the universe, and they provide one of the very few available constraints on physical conditions at that time. The first nucleosynthesis models were computed by Gamow (1948) and by Alpher & Herman (1949). Subsequent models have included modern nuclear reaction rates and accurate values for the background radiation field. The simplest big bang nucleosynthesis models assume that general relativity is valid at early times, that the universe is homogeneous and isotropic, and that only presently known forms of matter (baryons and leptons) and radiation were present. The recent nucleosynthesis calculations by Walker et al. (1991) assume only three species of light neutrinos and the recent measured value of 10.27 ± 0.08 minutes for the neutron half-life (cf. Byrne et al. 1990).

Comparison of our adopted value of $(\rm D/H)_p = (2.2\text{–}5.2) \times 10^{-5}$ with the Walker et al. calculations indicates that $\eta_{10} = 3.8\text{–}6.0$, where η_{10} is 10^{10} times the ratio of nucleons to photons by number. The ^{4}He abundance varies in the opposite sense to $(\rm D/H)_p$, because with increasing density at the time of nucleosynthesis deuterium will be more completely converted into ^{3}He and ^{4}He. Walker et al. find that the best estimate value of the primordial ^{4}He/H ratio by mass, $Y_p^{\rm obs}$, places η_{10} in the range 2.8–4.0, consistent with the value inferred from our adopted value of $(\rm D/H)_p = (2.2\text{–}5.2) \times 10^{-5}$. Pagel (1990) reaches a similar conclusion. This range in η_{10} leads to the important result that $0.06 \leq \Omega_B h_{50}^2 \leq 0.08$, where Ω_B is the baryon density in units of the Einstein-de Sitter closure density, and h_{50} is the Hubble constant in units of 50 km s^{-1} Mpc^{-1}. Should the Hubble constant be about 80 km s^{-1} Mpc^{-1} as current evidence suggests, then the deuterium data alone require that $\Omega_B = 0.023\text{–}0.031$.

If only presently known forms of matter exist, the basic assumptions of the big bang nucleosynthesis models are valid, and the cosmological constant is zero, then our results require an open universe. There are, however, both empirical and theoretical arguments that should be considered when discussing the evolution of the universe. In his recent discussion of the dynamical evidence for dark matter, Tremaine (1992) concludes that approximately 90% of the mass of the universe is in the form of dark nonbaryonic matter. This matter is located in the extended halos of galaxies, in clusters of galaxies, and perhaps elsewhere. Inflation models predict that the density parameter $\Omega = 1$. Also, Fowler (1990) argues that Ω_B approaching unity could be consistent with the measured light-element abundances if one relaxes the assumption of homogeneity and allows neutron diffusion between neutron-rich and neutron-poor regions in the early universe. Such models are not ruled out by our data. We can say on the basis of our data that if the early universe was homogeneous, then in order for Ω to equal unity the amount of nonbaryonic matter must be 14 times that of ordinary matter for $h_{50} = 1$ or 60 times for $h_{50} = 2$. Whether or not the expansion of the universe will eventually be stopped thus remains an open question.

5. FUTURE OBSERVATIONS

We have demonstrated that very accurate values of the D/H ratio and interstellar properties can be obtained for the Capella line of sight by analyzing the high-resolution and high S/N Lyα profile obtained with the GHRS echelle A grating. Our results are consistent with the hypothesis that the D/H ratio is constant in the Galactic disk as far as 1 kpc, but clearly this hypothesis should be tested by observing other lines of sight. Also, the uncertainties in our derived values for $N_{\rm H\,I}$ and $(\rm D/H)_{LISM}$ for the Capella line of sight could be reduced considerably by observing Capella near phase 0.75. At the present

time observations with echelle A are not feasible, but lower resolution observations with the G160M grating can accomplish this task with somewhat lower accuracy. We believe that this program should proceed. When it is built and launched, the *Lyman Far-Ultraviolet Spectrograph Explorer* (*FUSE*) will be able to sample more distant lines of sight by studying deuterium absorption in the higher members of the Lyman series.

This work was supported by NASA grant S-56500-D to the National Institute of Standards and Technology. A. Diplas and B. Savage acknowledge support from NASA grant NAG5-1852 to the University of Wisconsin-Madison. T. Ayres acknowledges support from NASA grants NAG5-199, NAG5-1215, and GO-2485.01-87A. We thank A. Dupree and E. Jenkins for providing us with the *Copernicus* observations of Capella, and J. Neff for providing the Lyα profile data for δ Lep. We also thank M. Shull and P. McCullough for carefully reading the manuscript and for their useful comments.

APPENDIX A

COMPARISON OF CAPELLA Lyα SPECTRA OBTAINED WITH THE GHRS AND THE *COPERNICUS* SATELLITE

As mentioned in § 3.3, the shape of the GHRS Lyα spectrum is inconsistent with published *IUE* spectra. The differences are not just in the depth of the deuterium line, which can be explained by the lower resolution ($R \approx 10{,}000$) of *IUE*, or the filling in of the hydrogen interstellar absorption feature, which can be explained by scattered light from the *IUE* echelle grating. The important difference is the overall shape of the stellar emission line, which can be characterized by the ratio of the red to blue peak flux and which should not be changed appreciably by either the lower resolution or the scattered light level in the *IUE* spectrum. Since the GHRS echelle and G140L low-dispersion spectra are consistent with each other, we have examined the *Copernicus* spectra of Capella as a consistency check. In parallel, Ayres et al. (1992) have obtained new *IUE* spectra of Capella and have reduced them and the archival spectra with a new analysis technique.

The *Copernicus* satellite obtained Lyα profiles of Capella at eight different times with a resolution of 20,000, intermediate between the *IUE* and GHRS echelle resolutions. These data were provided to us from the *Copernicus* archives by E. Jenkins and by A. Dupree. Table 7 summarizes the data and the measured peak ratios. The 1975 February 12 and 1976 January 18 profiles were analyzed by Dupree et al. (1977) and by McClintock et al. (1978). These data are noisy; however they do show red/blue peak ratios near 1.55 for most of the orbit, but ratios near 2.0 at phase 0.26–0.28. Much of the behavior can be simply explained as due to the maximum redshift of the Lyα profile of the G8 III star, which presumably has a narrower emission line than the more rapidly rotating G0 III star. The Mg II lines of the two stars show the same behavior (Ayres et al. 1983). The *Copernicus* red/blue peak ratio of the Lyα line at phase 0.26–0.28 is consistent with the GHRS ratio of 1.93 at phase 0.26.

APPENDIX B

POSSIBLE ABSORPTION FEATURES IN THE Lyα PROFILE

Figure 6*a* shows that the composite stellar line profile folded through the interstellar medium, for all plausible values of $N_{\rm H\,I}$, lies above the observed profile for a 0.1 Å region centered on 1215.29 Å. This difference, if it is real and not an artifact of our assumed intrinsic profiles, could be explained by an absorption line produced by gas in the interstellar medium or in the atmosphere of either star above where the Lyα line is formed. We are uncertain about the reality of this feature, because the observed deuterium line wing corrected for hydrogen absorption shown in Figure 4 does not show this feature. Also, there appears to be a similar discrepancy near 1215.6 Å for $N_{\rm H\,I} = 1.6$ and 1.8×10^{18} cm^{-2}. This could also indicate the presence of an absorption feature as previously mentioned in § 3.2.

We list in Table 8 spectral lines that could produce interstellar or circumstellar absorption near these wavelengths. Candidates include the Hβ doublet of He II, Fe II lines that pump fluorescent emission lines in cool giants (Carpenter et al. 1988), and the 14–0 vibrational transitions in the fourth positive band ($X^1\Sigma^+$–$A^1\Pi$) of CO (Kurucz 1976; Ayres, Moos, & Linsky 1981). The table lists

TABLE 7

SUMMARY OF *Copernicus* OBSERVATIONS

Day	Phase[a]	Blue Peak[b]	Red Peak[b]	Red/Blue
1976 Mar 10	0.26	34.59	71.59	2.07
1975 Jan 21	0.28	43.78	84.98	1.94
1974 Oct 19	0.37	57.10	81.65	1.43
1975 Feb 12	0.49	54.41	91.32	1.68
1976 Nov 2	0.53	47.36	72.02	1.52
1975 Mar 11	0.75	53.62	81.44	1.52
1976 Jan 18	0.76	39.84	59.72	1.50
1977 Oct 26	0.98	34.14	54.44	1.59

[a] Using the ephemeris cited by Ayres (1984, 1988).
[b] Counts per 14 s.

TABLE 8

CANDIDATES FOR THE 1215.29 AND 1215.6 Å ABSORPTION FEATURES

SPECTRAL FEATURE	REST FRAME WAVELENGTH (Å)			
	Of Laboratory	Of F Star	Of G Star	Of LISM
CO Q7	1214.807	1214.815	1215.035	1214.888
CO P6	1214.896	1214.904	1215.121	1214.977
CO R10	1214.923	1214.931	1215.148	1215.004
CO Q8	1214.963	1214.971	1215.188	1215.041
CO P7	1215.070	1215.078	1215.295	1215.151
He II Hβ	1215.09	1215.10	1215.32	1215.17
CO R11	1215.102	1215.110	1215.327	1215.183
CO Q9	1215.139	1215.147	1215.364	1215.220
He II Hβ	1215.17	1215.18	1215.40	1215.25
Fe II (3.15 eV)	1215.185	1215.193	1215.410	1215.266
T I Lyα	1215.230	1215.238	1215.455	1215.311
CO P8	1215.261	1215.269	1215.486	1215.342
CO R12	1215.298	1215.306	1215.523	1215.379
CO Q10	1215.334	1215.342	1215.559	1215.415
CO P9	1215.474	1215.482	1215.699	1215.555
Fe II (2.81 eV)	1215.503	1215.511	1215.728	1215.611
CO R13	1215.514	1215.522	1215.739	1215.595
CO Q11	1215.547	1215.555	1215.772	1215.628

the laboratory vacuum wavelengths for lines in the range 1214.8–1215.6 Å, and the wavelengths of these lines in the rest frames of the F star, the G star, and the LISM.

There are some coincidences between the wavelengths in Table 8 and the wavelengths of the possible absorption features at 1215.29 Å and near 1215.6 Å. Both Fe II lines are close matches if the lines are formed in the LISM, but the 3 eV excitation potential of the lower states in these transitions rules out this possibility. One of the He II lines lies near the 1215.29 Å line in the rest frame of the G star. This line is a plausible candidate since the Hα line of He II at 1640 Å is observed in Capella. There are several CO lines that lie close in wavelength to the absorption lines in the rest frames of both stars and the LISM. It is very likely that these CO lines are not formed in the LISM, since population of only the $J = 0$ and 1 levels has been detected so far in the line of sight toward ξ Per (Smith et al. 1991). On the other hand, absorption from high rotational levels is plausible in stellar spectra, since CO fourth positive lines are observed in the spectra of stars like the Sun and Arcturus, and pumping by the Lyα line has been identified as one of the mechanisms for producing fluorescent CO emission lines in this star (Ayres et al. 1981). Detailed calculations are needed to determine whether any of these lines should be present and why most of the CO lines are not present. Observations of Capella at phase 0.75 are critical to verifying the reality of the absorption features and the plausibility of these explanations.

While the He II and CO lines are plausible candidates, the most intriguing and unexpected possibility is interstellar tritium. The heaviest isotope of hydrogen, tritium, has a half-life of 12.3 yr, and is not anticipated to be present in the interstellar medium. Nevertheless, the excellent spectra for the Capella line of sight permit us to estimate its abundance for the first time. The tritium Lyα line is a doublet with vacuum wavelengths of 1215.2276 Å (for $J = \frac{1}{2}$ to $1\frac{1}{2}$) and 1215.2330 Å (for $J = \frac{1}{2}$ to $\frac{1}{2}$). Thus the lines are about -0.11 Å or -27 km s^{-1} relative to the deuterium lines. The data in Table 8 indicate that the tritium feature should be centered at 1215.311 Å in the rest frame of the LISM, very close to the absorption feature centered at 1215.29 Å. If future observations confirm that the absorption feature is real and the identification of tritium is correct, then the tritium column density would be $\sim 8.8 \times 10^{11}$ cm^{-2}, corresponding to a line center optical depth ~ 0.08 and the number ratio T/H $\sim 4.4 \times 10^{-7}$. We prefer a more conservative approach in which we take the above T/H ratio to be a 3 σ upper limit.

REFERENCES

Alpher, R. A., & Herman, R. C. 1949, Phys. Rev., 75, 1089
Anders, E., & Grevesse, N. 1989, Geochim. Cosmochim. Acta, 53, 197
Anderson, R. C. 1979, Ph.D. thesis, Johns Hopkins University
Anderson, R. C., Henry, R. C., Moos, H. W., & Linsky, J. L. 1978, ApJ, 226, 883
Anderson, R. C., & Weiler, E. J. 1978, ApJ, 224, 143
Ayres, T. R. 1979, ApJ, 228, 509
———. 1984, ApJ, 284, 784
———. 1988, ApJ, 331, 467
Ayres, T. R., Brown, A., Gayley, K. G., & Linsky, J. L. 1993, ApJ, 402, 000
Ayres, T. R., Moos, H. W., & Linsky, J. L. 1981, ApJ, 248, L137
Ayres, T. R., Schiffer, F. H., III, & Linsky, J. L. 1983, ApJ, 272, 223
Baliunas, S. L., & Dupree, A. K. 1979, ApJ, 227, 870
Basri, G. S. 1980, ApJ, 242, 1133
Basri, G. S., Linsky, J. L., Bartoe, J.-D. F., Brueckner, G., & Van Hooser, M. E. 1979, ApJ, 230, 923
Batten, A. H., Fletcher, J. M., & Mann, P. J. 1978, Publ. Dom. Astrophys. Obs., 15, 121
Batten, A. H., Hill, G., & Lu, X. 1991, PASP, 103, 623
Bertaux, J. L., Lallement, R., Kurt, V. G., & Mironova, E. N. 1985, A&A, 150, 1
Bobroff, N., Nousek, J., & Garmire, G. 1984, ApJ, 277, 678
Boesgaard, A. M., & Steigman, G. 1985, ARA&A, 23, 319
Bohlin, R. C., Savage, B. D., & Drake, J. F. 1978, ApJ, 224, 132
Brandt, J. C., et al. 1982, in The Space Telescope Observatory, ed. D. N. B. Hall (NASA CP-2244), 76
Bruhweiler, F. C. 1984, in Local Interstellar Medium, ed. Y. Kondo, F. C. Bruhweiler, & B. D. Savage (NASA CP-2345), 39
Bruhweiler, F. C., & Vidal-Madjar, A. 1987, in Exploring the Universe with the *IUE* Satellite, ed. Y. Kondo (Dordrecht: Reidel), 467
Bruston, P., Audouze, J., Vidal-Madjar, A., & Laurent, C. 1981, ApJ, 243, 161
Byrne, J., et al. 1990, Phys. Rev. Lett., 65, 289
Cardelli, J. A., Ebbetts, D. C., & Savage, B. D. 1990, ApJ, 365, 789
Cardelli, J. A., Savage, B. D., Bruhweiler, F. C., Smith, A. M., Ebbets, D. C., Sembach, K. R., & Sofia, U. J. 1991a, ApJ, 377, L57
Cardelli, J. A., Savage, B. D., & Ebbets, D. C. 1991b, ApJ, 383, L23
Carpenter, K. G., Pesce, J. E., Stencel, R. E., Brown, A., Johansson, S., & Wing, R. F. 1988, ApJS, 68, 345
Chassefiere, E., Dalaudier, F., & Bertaux, J. L. 1988, A&A, 201, 113
Clayton, D. D. 1985, ApJ, 290, 428
Cox, D. P., & Reynolds, R. J. 1987, ARA&A, 25, 303
Cruddace, R., Paresce, F., Bowyer, S., & Lampton, M. 1974, ApJ, 187, 497
Crutcher, R. M. 1982, ApJ, 254, 82
Delbourgo-Salvador, P., Audouze, J., & Vidal-Madjar, A. 1987, A&A, 174, 365
Duncan, D. K. 1992, Goddard High-Resolution Spectrograph Instrument Handbook, Version 3.0 (Space Telescope Science Institute)

Dupree, A. K., Baliunas, S. L., & Shipman, H. L. 1977, ApJ, 218, 361
Encrenaz, T., & Combes, M. 1983, Icarus, 52, 54
Ferlet, R., Lallement, R., & Vidal-Madjar, A. 1986, A&A, 163, 204
Fowler, W. A. 1990, in Baryonic Dark Matter, ed. D. Lynden-Bell & G. Gilmore (Dordrecht: Kluwer), 257
Frisch, P. C., & York, D. G. 1983, ApJ, 271, L59
Gamow, G. 1948, Phys. Rev., 74, 505
Gayley, K. G. 1992a, ApJ, 390, 573
———. 1992b, ApJ, 392, 353
Geiss, J., & Reeves, H. 1981, A&A, 93, 189
Gry, C., Lamers, H. J. G. L. M., & Vidal-Madjar, A. 1984, A&A, 137, 29
Gry, C., Laurent, C., & Vidal-Madjar, A. 1983, A&A, 124, 99
Gry, C., York, D. G., & Vidal-Madjar, A. 1985, ApJ, 296, 593
Henry, R. C., et al. 1991, BAAS, 23, 903
Hubbard, W. B., & MacFarlane, J. J. 1980, Icarus, 44, 676
Jenkins, E. B., Savage, B. D., & Spitzer, L. 1986, ApJ, 301, 355
Kalberla, P. M. W., Mebold, U., & Reich, W. 1980, A&A, 82, 275
Kulkarni, S. R., & Heiles, C. 1987, in Interstellar Processes, ed. D. H. Hollenbach & H. A. Thronson, Jr. (Dordrecht: Reidel), 87
Kurucz, R. L. 1976, Smithsonian Astrophys. Obs. Spec. Rep., No. 374
Lallement, B., Vidal-Madjar, A., & Ferlet, R. 1986, A&A, 168, 225
Laurent, C. 1983, in Proc. ESO Workshop on Primordial Helium, ed. P. A. Shaver, D. Kunth, & K. Kjar (Garching: ESO), 335
Lubowich, D. A., Anantharamaiah, K. R., & Pasachoff, J. M. 1989, ApJ, 345, 770.
McClintock, W., Henry, R. C., Linsky, J. L., & Moos, H. W. 1978. ApJ, 225, 465
McCullough, P. R. 1992, ApJ, 390, 213
McCullough, P. R., Heiles, C., & Glassgold, A. E. 1991, BAAS, 23, 933
Morton, D. C. 1991, ApJS, 77, 119
Murthy, J., Henry, R. C., Moos, H.W., Landsman, W. B., Linsky, J. L., Vidal-Madjar, A., & Gry, C. 1987, ApJ, 315, 675
Murthy, J., Henry, R. C., Moos, H. W., Vidal-Madjar, A., Linsky, J. L., & Gry, C. 1990, ApJ, 356, 223 Erratum 1991, ApJ, 378, 455
Neff, J. E., Landsman, W. B., Bookbinder, J. A., & Linsky, J. L. 1990, in Evolution in Astrophysics (ESA SP-310), 341
Pagel, B. E. J. 1990, in Baryonic Dark Matter, ed. D. Lynden-Bell & G. Gilmore (Dordrecht: Kluwer), 237
Paresce, F. 1984, AJ 89, 1022
Pasachoff, J. M., & Vidal-Madjar, A. 1989, Comments Astrophys., 14, 61
Rogerson, J. B., & York, D. G. 1973, ApJ, 186, L95
Shore, S. N. 1990, GHRS System Engineering Rep. GHRS-SV-28
Shore, S. N., Ferrini, F., & Palla, F. 1987, ApJ, 316, 663
Smith, A. M., et al. 1991, ApJ, 377, L61
Spitzer, L., Jr. 1978, Physical Processes in the Interstellar Medium (New York: Wiley), 27
Steigman, G., & Tosi, M. 1992, preprint
Tremaine, S. 1992, Phys. Today, 45, No. 2, p. 28
Van Steenberg, M. E., & Shull, J. M. 1988, ApJ, 330, 942
Vidal-Madjar, A. 1977, in The Solar Output and its Variation, ed. O. R. White (Boulder: Colorado Associated Univ. Press), 224
Vidal-Madjar, A., Laurent, C., Bruston, P., & Audouze, J. 1978, ApJ, 223, 589
Walker, T. P., Steigman, G., Schramm, D. N., Olive, K. A., & Kang, H.-S. 1991, ApJ, 376, 51
Welsh, B. Y. 1991, ApJ, 373, 556
York, D. G., & Frisch, P. C. 1984, in IAU Colloq. 81, Local Interstellar Medium, ed. Y. Kondo, B. C. Bruhweiler, & B. D. Savage (NASA CP-2345), 51